Electronic structure and molecular motions of the quasi-one-dimensional organic conductor $(naphthalene)_2AsF_6$

A. Kaiser and E. Dormann
Physikalisches Institut, Universität Karlsruhe, D-76128 Karlsruhe, Germany
(Received 7 May 2004; revised manuscript received 27 August 2004; published 14 March 2005)

We present high-resolution ^{13}C nuclear magnetic resonance spectra, and frequency-dependent ^{1}H and ^{19}F nuclear spin relaxation data for the quasi-one-dimensional organic conductor $(NA)_2AsF_6$, the radical cation salt of a pure aromatic hydrocarbon with the highest Peierls transition temperature, compared, e.g., with fluoranthene (FA), pyrene (PY), and perylene (PE) salts. The spin density distribution on the radical cation is unravelled, and the decrease of the conduction electron density of state at the Peierls transition is reflected by the variation of the ^{13}C line shift as well as the proton spin-lattice relaxation with decreasing temperature. In spite of its poor chemical stability, this organic conductor exhibits diffusive decay of long wavelength conduction electron spin correlations up to $\tau^*=0.72$ ns at 240 K. The fluorine and proton spin-lattice relaxation rate reveals the temperature-dependent slowdown of the rotation of the anion octahedra. A correlation between the occurance of the Peierls transition of the radical cation salts and the slowdown of the anion rotation is supported by these results of $(NA)_2AsF_6$, compared with $(PY)_{12}(SbF_6)_7$, $(FA)_2AsF_6$, and $(FA)_2SbF_6$. The correlation time of the anion rotation at the Peierls transition temperature $\tau_c(T_P)$ barely differs for different radical cation salts with the same anions in spite of differing T_P value.

DOI: 10.1103/PhysRevB.71.115108 PACS number(s): 71.20.Rv, 76.60.Cq, 76.60.Es, 76.70.−r

I. INTRODUCTION

The electrochemical growth of needlelike naphthalene ($C_{10}H_8$, abbreviated as NA) radical cation salt crystals of the composition $(NA)_2X$, $X=PF_6$, AsF_6, by anodic oxidation of the aromatic hydrocarbon molecule NA in dichloromethane (CH_2Cl_2) solution in the presence of the appropriate complex anion X opened the door to a large family of quasi-one-dimensional organic conductors.[1] In the years that followed, salts of fluoranthene,[2] pyrene,[3] perylene,[4] and many others were presented, with various stoichiometries and structural arrangements of the aromatic molecules (arenes).[5] These occasionally delicate solids allowed the study of charge density wave (CDW) transport and the corresponding high temperature CDW fluctuations,[6–8] and the Peierls transition as revealed by diffuse x-ray scattering,[9,10] by microwave conductivity,[11–13] or by static magnetic susceptibility.[13–15] All these radical cation salts show stacks of flat, parallel-packed arene molecules, arranged with the general rule of optimizing π-electron molecular-orbital (MO) overlap. The closed shell diamagnetic counterions X^-, such as PF_6^-, AsF_6^-, ClO_4^-, BF_4^-, or others, determine, via the stoichiometry of the salt, the band filling of the one-dimensional conduction band, extended in the stacking direction. The negligible spin orbit coupling of the electron spin in a π-molecular orbital of a molecule that is built up only from the light elements carbon ($Z=6$) and hydrogen, and the strict one dimensionality of the motion of the conduction electron in the conduction band built up from such MOs, give rise to an extremely slow spin-lattice relaxation of these conduction electrons.[16] Unusually narrow electron spin resonance (ESR) lines for these arene radical cation salts have been reported already from early experiments.[17–19] Thus these conductors allowed for quite a number of applications[20–22] as well as the development of a remarkable number of techniques for their characterization, including various types of ESR imaging.[23–27] In this regard, it is surprising, that the prototype of all these arene radical cation salts, the naphthalene salt, has not been studied in any further detail, except for the original chemical report[1] and a more detailed ESR analysis.[19,28] This is possibly due to the early report of the instability of these single crystals at temperatures above −30 °C, their naphthalene smell in air, and the gradual recrystallization of naphthalene accompanying sample decomposition already below 65–70 °C.[1] We showed recently that the static magnetic susceptibility of $(NA)_2AsF_6$ can be analyzed quantitatively, nevertheless.[15] Less than 1×10^{-3} Curie paramagnetic defects per formula unit were found. The Peierls transition at $T_P=234\pm4$ K remained well defined, even if the extrapolated value of the Pauli paramagnetism related to the weight corresponding to one mole of $(NA)_2AsF_6$ varied by 40% within 5 weeks. Therefore, we present here a detailed nuclear magnetic resonance (NMR) analysis of $(NA)_2AsF_6$. The unpaired spin density distribution in the NA radicals is derived by ^{13}C high-resolution NMR (with proton cross polarization and magic angle spinning, abbreviated as CP-MAS),[23] studied in dependence of the temperature. The degree of one dimensionality of the conduction electron spin dynamics in the high-temperature metallic phase of $(NA)_2AsF_6$ above T_P is characterized by the investigation of the temperature and the frequency dependence of the modified Korringa relaxation[16,29] of the NA protons. In relation to the typically rather short intrastack scattering times of the conduction electrons of arene radical cation salts of about $\tau_\parallel=3$–17 fs,[30,31] the time constant $\tau^*=0.72$ ns derived for the typical end of the diffusive decay of the long wavelength spin density wave excitations at $T=240$ K, i.e., $\tau^*:\tau_\parallel\approx10^5:1$, gives ample evidence for the classification of

$(NA)_2AsF_6$ as a quasi-one-dimensional conductor.

A multiple role is played by the complex anions in conducting radical cation salts.[1,5,16,23,32] First of all, the diamagnetic, single charged anions such as PF_6^-, or ClO_4^- determine the conduction band filling via the stoichiometry of the respective salt. Stoichiometries ranging between 6:1 and 4:3 were reported.[5] But the complex anions play also a crucial role for the formation of the various groundstates that can be reached via temperature, magnetic field, and pressure, especially for cations also incorporating Se or S atoms in their molecular units, e.g., metallic, charge density wave ordered, spin density wave ordered, spin-Peierls distorted, antiferromagnetically ordered, or superconducting.[16,33] Especially noncentrosymmetric anions such as ClO_4^- are efficient in inducing structural phase transitions via the variable degree of their orientational order.[34] But also centrosymmetric, only slightly distorted octahedral anions such as PF_6, AsF_6, and SbF_6 play a rather relevant role in the radical cation salts of simple arenes for the appearance of structural phase transitions, and especially the three-dimensional (CDW) Peierls transition.[3,35,36] In the high-temperature metallic phase of these quasi-one-dimensional organic conductors independent CDW fluctuations on the individual conductive arene stacks are observed. Interstack coupling is weak, and according to the relative phase of the locked-in CDWs in the ordered low-temperature Peierls distorted phases studied by now, phononlike and Coulomb coupling between neighboring CDWs must be of comparable importance.[9,10,16,37] Actually, doubling of the unit cell perpendicular to the stacking direction, influencing the CDW fluctuations, was observed by x rays already at temperatures approaching the Peierls transition temperature.[9,10] For the transverse coupling, the hexafluoride anions seem especially important, because they rotate at elevated temperature but are squeezed between the neighboring conducting stacks at lowered temperature (see Fig. 1). Because the radical cations' charge influences the bond lengths of the arene, as was proved for perylene radicals by experiment and model calculations,[38] transverse charge density coupling may be mediated by arene-hexafluoride-arene interaction.

In x-ray crystal structure analysis primarily large standard deviations and pronounced thermal ellipsoids of the F atoms reflect the rotational motions of the hexafluoride anions at room temperature.[3,39] NMR relaxation of ^{19}F and ^{1}H nuclei is an especially useful probe for monitoring the freezing-in of the anion rotational motion with lowering of the temperature.[36,40,41] This is due to several favorable facts; Both isotopes, ^{1}H and ^{19}F, have 100% abundance, nuclear spin $I=1/2$, and large gyromagnetic ratios, thus both can easily and separately be measured by NMR in a fixed external magnetic field. The well-known distance and orientation dependence of ^{1}H-^{1}H, ^{19}F-^{19}F, and ^{1}H-^{19}F dipolar magnetic interaction can thus be exploited, and separated, in NMR relaxation studies.[42] The librational motions of the arene radicals are reflected by the ^{1}H-^{1}H contributions, the hexafluoride rotational jumps by the ^{19}F-^{19}F contributions, and the combined arene-anion motions by the ^{1}H-^{19}F contributions to the nuclear spin-lattice relaxation.[42,53] Thus, NMR relaxation reflects the squeezing of the hexafluoride anions between the cation stacks and the formation of C-H$\cdots$F bonding contributions accompanying the thermal lattice contraction. We have suggested as a generalizable rule that hexafluoride anion rotation is slowed down to the NMR accessible time scale of some hundred MHz before the three-dimensional Peierls transition is really locked-in.[36] This suggested qualitative picture will be tested critically in this investigation for the arene radical cation salt with the highest Peierls transition temperature, i.e., $(NA)_2AsF_6$.[1,15,19]

This paper is organized as follows. The experimental section, Sec. II, summarizes the relevant measuring details (II A) and presents our main experimental results (II B). The ^{13}C Knight shift is derived and analyzed quantitatively in Sec. III A. It yields the spin density distribution and temperature-dependent conduction electron susceptibility of $(NA)_2AsF_6$. Spin-lattice relaxation (^{1}H, ^{19}F) is analyzed in Sec. III B. Based on these two sections, our experimental results are discussed in Sec. IV. For $(NA)_2AsF_6$, the degree of one dimensionality of the conduction electron spin dynamics is derived from the NMR data (Sec. IV A). The role played by slowing down of the anion rotation for the Peierls transition is discussed in Sec. IV B. Important results of our work are summarized in Sec. V.

II. EXPERIMENTAL RESULTS

A. Measurement details

The $(NA)_2AsF_6$ crystals were grown by anodic oxidation of a solution of naphthalene and the tetrabutylammonium salt of hexafluoroarsenate in CH_2Cl_2 at $T=-40$ °C.[1,15] The grown samples were stored in an inert atmosphere in a freezer at -17 °C until used. High-resolution variable-temperature NMR spectra of ^{13}C were recorded at 7 T field strength ($\nu_P=300$ MHz, $\nu_C=75.4$ MHz), using proton enhancement, proton decoupling (occasionally gated), and MAS up to $\nu_{rot}=15$ kHz (Figs. 2 and 3). Liquid impurity phases are separated by centrifugal forces and thus are of no importance for these spectra. For measurements of ^{1}H and ^{19}F spin-lattice relaxation the samples were enclosed in a glass crucible in order to prevent free vaporization and contact with air. Fourier transform spectra had to be analyzed during the course of the proton inversion-recovery T_1 measurements, because the contribution of solvent inclusions in pores and cracks of the crystals gives rise to narrow line liquid signals at temperatures above the CH_2Cl_2 melting point and Pake doublets at low temperatures that definitely have to be separated on account of their different $T_1(T,\nu)$ dependences (Fig. 4). The larger ^{1}H and ^{19}F Larmor frequencies, i.e., 300 MHz for ^{1}H, 282 MHz for ^{19}F, and 53 MHz for both were realized with a 7 T superconducting magnet and a variable field electromagnet ($\leqslant$1.4T). For measurements at $\nu_P=14$ MHz, the time dependence of the proton-related Overhauser shift of the conduction electron ESR line ($\nu_e=9.5$ GHz) could be used, allowing the analysis of individual single crystals, a better signal-to-noise ratio, and an unambiguous separation of those protons that interact with the conduction electrons (thus not originating from decomposed crystals and solvent molecules included in the crystals). The inset of Fig. 5 shows that proton-$T_{1\rho}$ data are indispensable

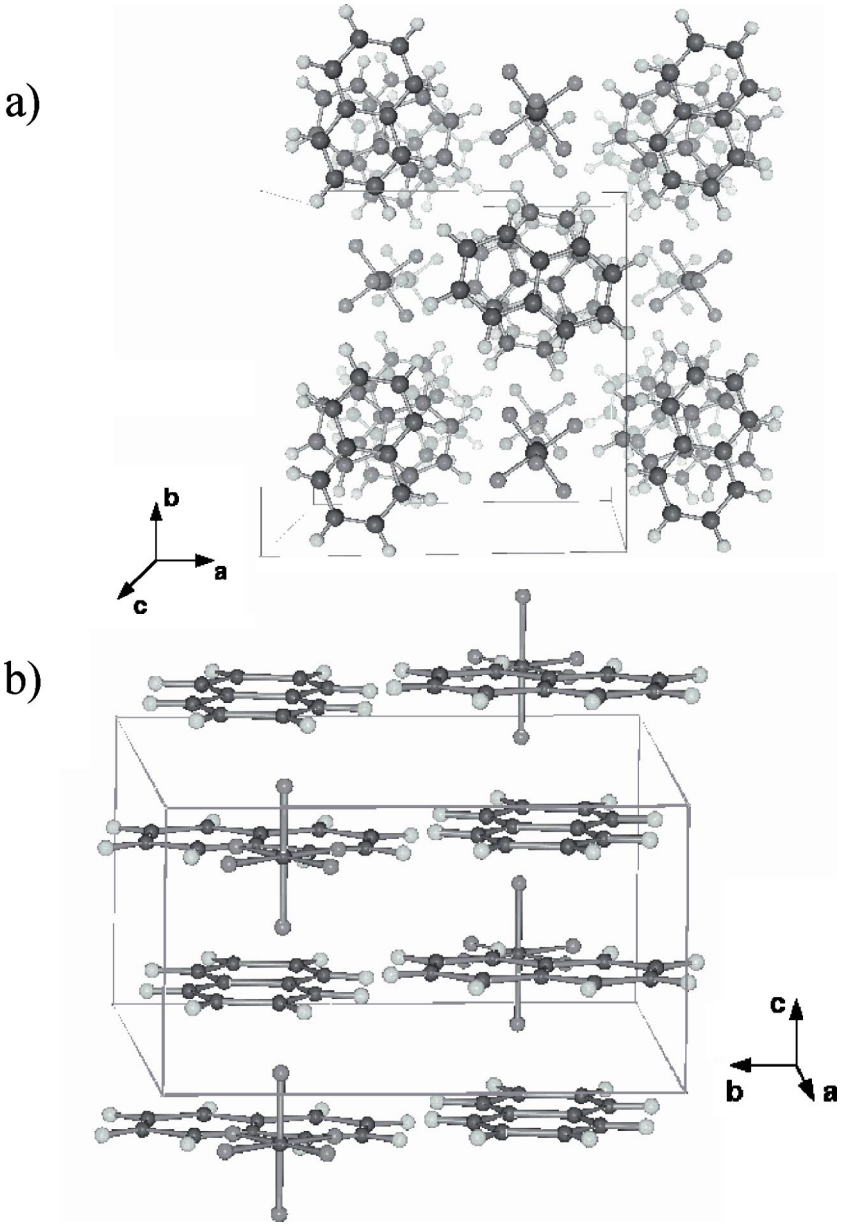

FIG. 1. Crystal structure of $(NA)_2X$. Molecular packing for $X=PF_6$ seen along the stacking axis c (a) and along the *a* axis (b).

in narrowing down the frequency dependence of proton T_1^{-1}. These rotating frame results were recorded at $\nu_P=300$ MHz. The error limit of the T_1^{-1} data is estimated to be about 10%, typically.

B. Results

1. ^{13}C-NMR line shift

Figure 2 shows the temperature dependence of ^{13}C-CP-MAS spectra of $(NA)_2AsF_6$. The dependence of the spectra on MAS-rotation frequency was analyzed in detail. For the high rotation frequency used for recording the spectra shown in Fig. 2, spinning side bands are only of negligible importance and thus not indicated in the figure. Gated decoupling was used to discriminate the proton-bound positions C1–C8 from the inner position C9 and C10. (For numbering see Fig. 6.[43]) Figure 3 shows the variation of the spectra that result from gated decoupling of the protons at $T=240$ K, which reveals clearly the distinct behavior of line *A* compared to *B* and *C*. Figure 6 summarizes the temperature dependence of the ^{13}C line shift obtained from two different samples.

2. Proton spin relaxation in metallic phase

Figure 5 collects the relevant high temperature results concerning temperature and frequency dependence of ^{1}H spin-lattice relaxation of $(NA)_2AsF_6$. Whereas the high-frequency data are dominated by the typical $\omega^{-1/2}$ behavior of one-dimensional (1D) conductors, the low-frequency (rotating frame) results reveal the limit of (1D) spin dynamics.

3. ^{19}F and ^{1}H low-temperature spin-lattice relaxation

For the low-temperature range, the temperature dependences of the fluorine spin-lattice relaxation rate measured at

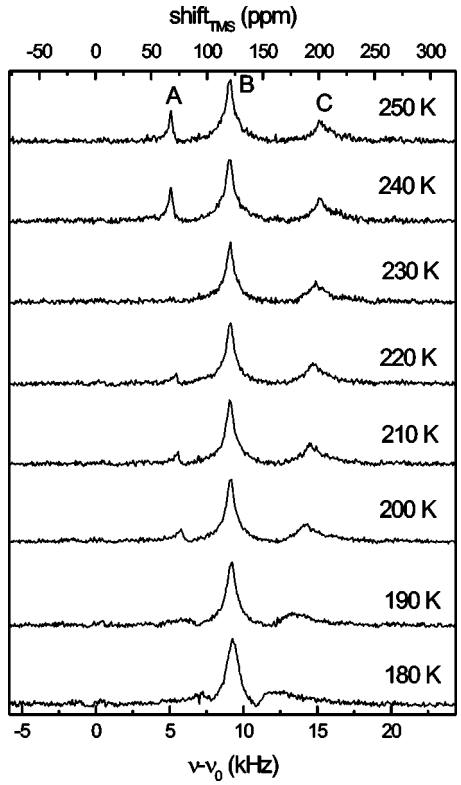

FIG. 2. ^{13}C-CP-MAS NMR spectra of $(NA)_2AsF_6$ as function of temperature, with labeling of the lines used in text. (Frequency and shift relative to tetramethylsilane, TMS; ν_{rot}=10 kHz.)

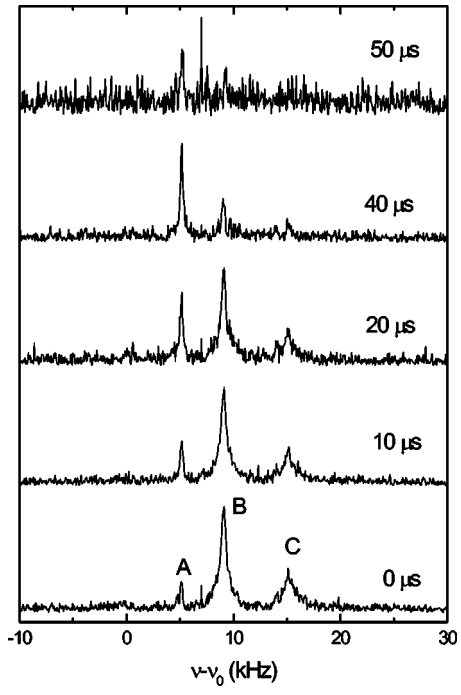

FIG. 3. Influence of gated decoupling on ^{13}C-CP-MAS spectra of $(NA)_2AsF_6$ (T=240 K, ν_{rot}=9 kHz).

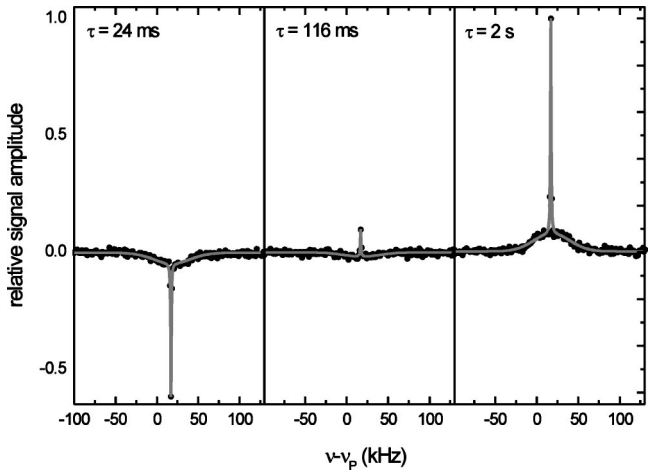

FIG. 4. Variation of the proton NMR spectrum of a $(NA)_2AsF_6$ sample during inversion-recovery sequence (ν_P=300 MHz, T =240 K). The solid line fit shows the separation in a broad Gaussian line of $(NA)_2AsF_6$ protons and a narrow Lorentzian line of solvent inclusions.

two different Larmor frequencies of 53 and 282 MHz are shown in Fig. 7. Two maxima of the rate can be seen, which have a frequency dependence typical for motion-induced relaxation of nuclear spins described in the Bloembergen-Purcell-Pound (BPP) model.[44]

The results of proton T_1 measurements at 53 and 300 MHz are collected in Fig. 8. Here the two frequency-dependent maxima of the rate, explainable by the BPP

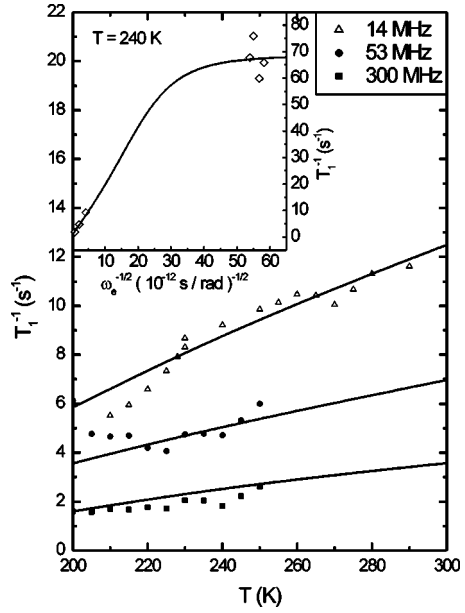

FIG. 5. Temperature dependence of the proton nuclear spin-lattice relaxation rate for different proton Larmor frequencies $\nu_p = \omega_p/(2\pi)$ in $(NA)_2AsF_6$. The inset shows the frequency dependence of $T_1^{-1}(^1H)$ at T=240 K, including low-frequency $T_{1\rho}$ data on an $\omega_e^{-1/2}$ scale ($\omega_e = \omega_p \gamma_e/\gamma_p$). The solid line fits are explained in Sec. III B. The approximate linearity of the fit is misleading; it results from accidental smoothening of several strongly T-dependent contributions.

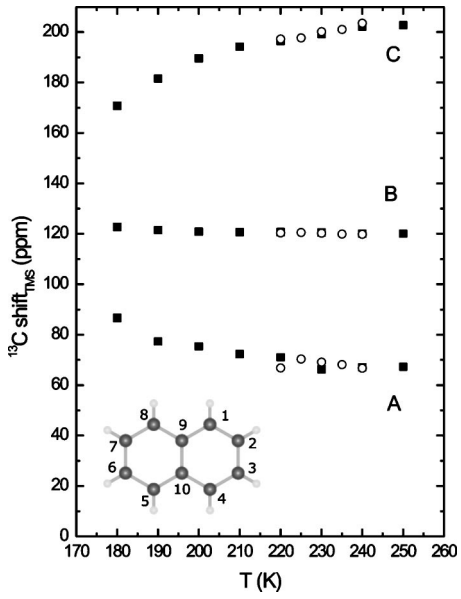

FIG. 6. ^{13}C-CP-MAS NMR line shifts for two different samples (open and filled symbols) relative to TMS versus temperature for $(NA)_2AsF_6$. The inset shows the numbering of the carbon positions in the NA radical cation used in this paper. *A*, *B*, *C*: see Figs. 2 and 3.

model, are less pronounced. The fluorine and the proton spin-lattice relaxation rates show frequency-dependent offsets, which are substantially larger for the lower Larmor frequencies. These additional relaxation contributions are the typical consequence of the spin diffusion to relaxing paramagnetic defects and impurities.[40,45] They do not interfere with the quantitative analysis of the BPP-like relaxation maxima performed below. These impurities are less efficient in the metallic phase, shown in Fig. 5.

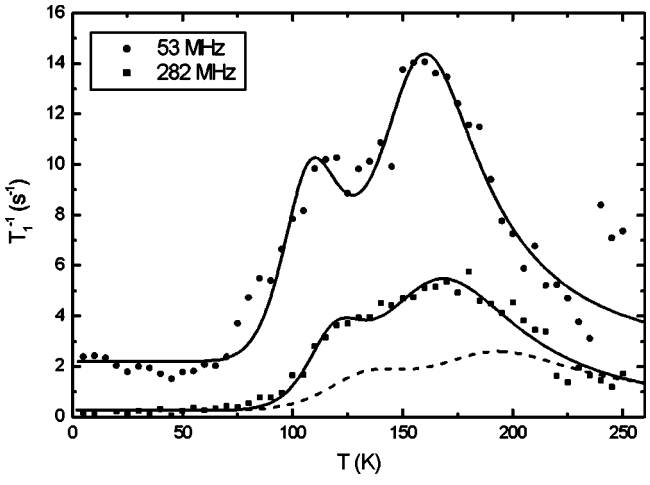

FIG. 7. Temperature dependence of the spin-lattice relaxation rate T_1^{-1} of the fluorine nuclei at the Larmor frequencies of 53 and 282 MHz. The solid lines are the separate fits with the BPP model; the broken line shows the fit with the fit parameters of 53 MHz adopted for 282 MHz. (See Sec. III B 3 and Table II.)

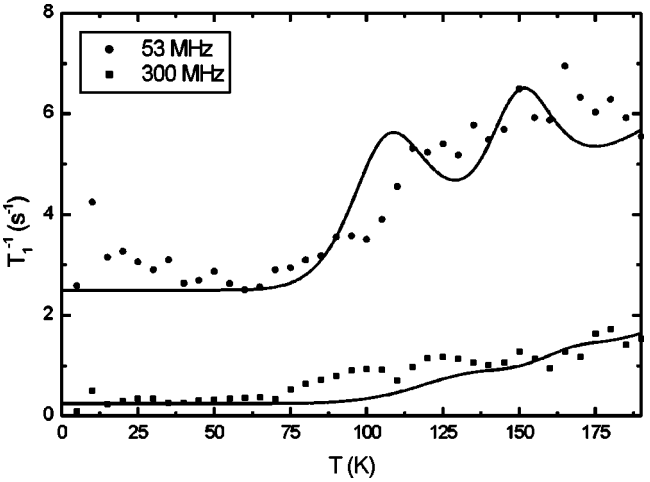

FIG. 8. Temperature dependence of the spin-lattice relaxation rate T_1^{-1} of the protons at Larmor frequencies of 53 and 300 MHz. The fits shown as solid lines are simultaneous fits of both frequencies using for the fluorine proton interaction the same parameters gained by the fit of the fluorine rate. (For details see Sec. III B 3.)

III. ANALYSIS

A. Knight shift and temperature dependence of conduction electron susceptibility

1. Relation between Knight shift and C-site-specific spin density

The local, temperature-dependent isotropic Knight shift can be calculated from[46–48]

$$K_i(T) = a_i \chi_{ce}(T)/(\hbar \gamma_e \gamma_C N_A), \tag{1}$$

with the temperature-independent, isotropic, hyperfine coupling constants a_i at the molecular carbon site i (Fig. 6), γ_e and γ_C the conduction electron and ^{13}C nuclear spin gyromagnetic ratio, and χ_{ce}/N_A the Pauli paramagnetic susceptibility per $(NA)_2^{+\bullet}$ dimer. A first order estimate of the coupling constants a_i is obtained from the HOMO (highest occupied molecular orbital) spin densities[49] (numbers presented in second column of Table I) with the Karplus-Fraenkel relation,[50]

$$a_i/2\pi = Q\rho_i + \sum_j Q_N \rho_j, \tag{2}$$

with Q=99.7 MHz for C1–C8, Q=85.4 MHz for C9 and C10, and Q_N=−38.9 MHz with ρ_j the spin densities of the respective nearest C neighbors to site i. These data, compiled in Table. I, are used to calculate the theoretical value of the Knight shift, $K_{i,t}$ for $\chi_{ce}=100\times10^{-6}$ emu/mole, a typical value for arene radical cation salts. A comparison with the well-known isotropic ESR proton hyperfine coupling constants of the naphthalene radical anion, i.e., 4.90 G and 1.83 G (Ref. 51), yields 20% deviation in the ρ_i values, but only 6% deviation in their ratio. The main weakness of the extended Hückel HOMO spin densities is the absence of polarization effects that give rise to negative unpaired spin densities, but the $K_{i,t}$ estimates certainly can help for the site assignment.

TABLE I. Spin densities ρ_i, hyperfine coupling constants a_i, and Knight shifts K_i for ^{13}C in $(NA)_2AsF_6$. *t*, HOMO values (Ref. 49) and *m* experimental results.

Position	$\rho_{i,t}$	$a_{i,t}$(MHz)	$K_{i,t}$(ppm)[a]	$a_{i,m}$(MHz)	$\rho_{i,m}$
C1,C5	0.089	+46.3	+61.6		
				+53.4±1.5	+0.092±0.001
C4,C8	0.091	+48.5	+64.6		
C2,C6	0.038	−6.3	−8.4		
				−4.2±0.4	+0.048±0.001
C3,C7	0.034	−10.3	−13.8		
C9,C10	0.0	−43.8	−58.4	−32.7±1.8	−0.031±0.001

[a]Calculated for $\chi^m_{ce}=100\times10^{-6}$ emu/mole.

2. Correlation between temperature dependence of Knight shift and susceptibility

The highly resolved ^{13}C-CP-MAS spectra of $(NA)_2AsF_6$ are shown for different temperatures in Fig. 2 relative to the TMS standard. The three lines in the spectra are labeled as *A*, *B*, and *C*. The absolute value of the Knight shift, i.e., the line shift related to the spectral line position of neutral naphthalene molecules, decreases with decreasing temperature. The center of gravity of line *B* is only shifted by −2.7 ppm at 240 K relative to neutral naphthalene. The lines *A* and *C* move with decreasing temperature towards line *B*. The gated decoupling measurement indicates that line *A* results from the non-proton-bound carbon sites C9 and C10. (See Figs. 3 and 6.) The HOMO spin densities, which are connected via the Karplus-Fraenkel relation [Eq. (2)] with the isotropic hyperfine interaction constants, predict five lines in the ^{13}C spectra. The reason why only three lines are observable in the highly resolved ^{13}C spectra is that two times two lines overlap in the spectra and build one single line (Table I). This explanation is supported by the ratio of the line areas between lines *A* and *C*. Thus all carbon sites of the naphthalene molecule could be assigned with a line in the spectra.

The temperature dependence of the ^{13}C line shift relative to the TMS standard shown in Fig. 6 is not linear. This is not unexpected, because the Knight shift is proportional to the magnetic conduction electron susceptibility and the susceptibility does not behave as the Pauli susceptibility of a three-dimensional metal, but shows a rapid decrease with decreasing temperature. This is a consequence of the appearance of the Peierls transition, which was observed for different samples in the temperature range between 230 and 240 K.[15] The Knight shift in Fig. 6 is not proportional to the average magnetic conduction electron susceptibility measured recently using a SQUID (superconducting quantum interference device) magnetometer for polycrystalline samples.[15] The samples used for both NMR and SQUID measurements contain many crystals of the radical cation salt and a part of these crystals are aged or decomposed. The early report already mentioned vaporization and recrystallization of the naphthalene molecules.[1] These effects in the ^{13}C spectra are visible as the higher signal intensity of line *B* that appears close to the spectral position of neutral naphthalene.

Fortunately, the Knight shift of the ^{13}C lines is a measure of the intrinsic conduction electron susceptibility. [See Eq. (1).] In fitting the intrinsic susceptibility, an exponential law[14] with the effective band gap as parameter was used for the low-temperature region below the Peierls transition, while the Lee-Rice-Anderson (LRA) model[52] with the limiting value of the Pauli susceptibility and the mean field temperature as parameters was used for temperatures around the Peierls transition and above. The result is shown in the right part of Fig. 9. In terms of this intrinsic susceptibility of the conduction electrons the so-called Jaccarino Clogston plot shows the linear correlation between the susceptibility and the Knight shift. (See the left part of Fig. 9.) The extrapolation of the line positions to zero conduction electron susceptibility confirms that the position of the three lines lies inside the ^{13}C linewidth of neutral naphthalene molecules measured with the same measuring technique.[43]

The slope of the lines *A* to *C* in the Jaccarino-Clogston plot are a measure for the isotropic hyperfine coupling constants $a_{i,m}$ at the different carbon sites. (See Table I.) The unambiguous assignment of the ^{13}C-NMR lines to the carbon sites allows us to calculate the spin densities on the naphthalene molecule from the measured isotropic hyperfine interaction constants using the Karplus-Fraenkel relation. (See Table I.) The highest value of the spin density is found at the carbon atoms C1, C4, C5, and C8. (For the notation, see Fig.

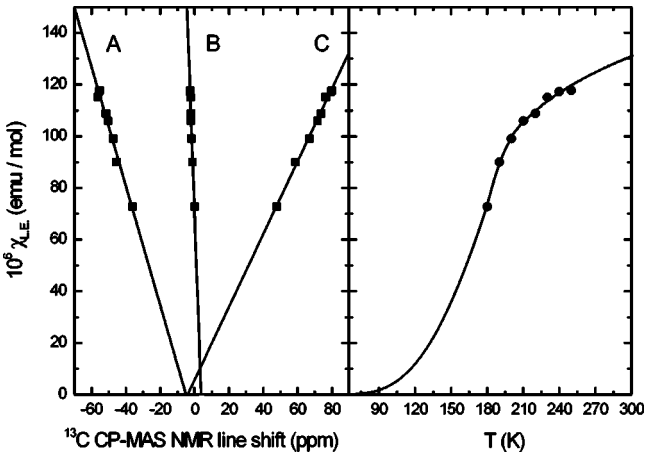

FIG. 9. Correlation of the temperature-dependent conduction electron magnetic susceptibility (right part) and ^{13}C-CP-MAS NMR line shift relative to neutral NA for $(NA)_2AsF_6$ with the temperature as an implicit parameter (left part).

6.) Each second naphthalene molecule in the stack is rotated by 90° (Fig. 1) such that the overlap of the wave functions at the four mentioned carbon sites is the largest. Thus it seems reasonable that the highest values of the spin density occurs at these four carbon sites.

B. Nuclear spin-lattice relaxation

Nuclear spin-lattice relaxation for ^{1}H and ^{19}F nuclei $\left(I=\frac{1}{2}\right)$ in arene radical cation salts such as $(NA)_2AsF_6$ is dominated by the paramagnetic defects in the lowest temperature range, by the thermally activated anion rotations, and the possibly accompanying arene librational motions in the intermediate range, and—only for the protons—by the hyperfine interaction with the conduction electrons in the metallic high-temperature phase above the Peierls transition temperature. Since $\chi(T)$ of the conduction electrons just has been determined (Fig. 9), their contribution can as well be calculated for $T>T_P$ as $T<T_P$. The appropriate expressions for the theoretical descriptions of these contributions have been reported already, so we refer to these sources and present only the definitions of the parameters derived from experiment.

1. Modeling of the low-temperature data

The influence of the AsF_6 anion rotation is described in the framework of the Bloembergen-Purcell-Pound (BPP) model.[42,44] The spectral densities of the relevant dipole-dipole interactions are approximated by Lorentzian functions

$$J(\omega)=\tau_c/[1+(\omega\tau_c)^2] \tag{3}$$

with the respective correlation times τ_c varying with temperature according to a simple Arrhenius law

$$\tau_c=\tau_\infty\exp(E/k_BT). \tag{4}$$

Modulations of ^{19}F-^{19}F orientations in the anion octahedra as well as the modulation of the ^{19}F-^{1}H separations due to AsF_6 rotational jumps have to be considered. Regarding the protons the modulation of ^{19}F-^{19}F is replaced by a modulation of ^{1}H-^{1}H orientations in the NA molecules by their librational motion. We use two indices for the adjusted activation energies E, correlation times τ_∞, and relaxation strength parameters K.[36,40,41] The influence of the ^{19}F-^{19}F interaction on the ^{19}F spin-lattice relaxation rate is thus parametrized as

$$T_{1,FF}^{-1}=K_{FF}[J(\tau_{FF},\omega_F)+4J(\tau_{FF},2\omega_F)], \tag{5}$$

whereas the contribution of the ^{19}F-^{1}H interaction for ^{19}F is

$$T_{1,FH}^{-1}=K_{FH}\{J[\tau_{FH},(\omega_F-\omega_H)]+3J(\tau_{FH},\omega_F)+6J[\tau_{FH},(\omega_F+\omega_H)]\}. \tag{6}$$

The total spin-lattice relaxation rate of ^{19}F nuclei is thus described by

$$T_{1,F}^{-1}=T_{1,FF}^{-1}+T_{1,FH}^{-1}+T_{1,FD}^{-1}, \tag{7}$$

where the last contribution takes the diffusion to localized paramagnetic defects and impurities into account.[45,53–57] (Analogous expressions are used for the proton-proton (HH) and proton-fluorine (HF) contributions.)

2. Modeling of the conduction electron Korringa-like contribution for the protons

AsF_6 is a diamagnetic closed shell complex anion which is not influenced by the conduction electrons' density of states. The conduction electrons interact strongly with the ^{13}C and ^{1}H nuclei of the naphthalene radical cations, however. The susceptibility of the conduction electrons below and above T_P is temperature dependent but known from Fig. 9 experimentally. The modification of the Korringa relaxation known from ordinary three-dimensional metals[42] for one-dimensional metals was treated theoretically 25 years ago.[16,23,29,48] For a one-dimensional (1D) metal, only $q\approx 0$ and $q\approx 2k_F$ conduction electron scattering contributions are possible, which have to be treated separately. Due to the slow, diffusive decay of the long wavelength SDW excitations, the $q=0$ part of the relaxation rate is frequency-dependently enhanced up to the huge factor $(\tau^*/\tau_\parallel)^{1/2}$, where τ^* is the shorter one of $\tau_\perp$, the transversal hopping time of the conduction electron, and τ_{ce-d}, which is the time needed for the conduction electron to encounter a relaxing defect on its own stack during the 1D motion. Thus, the conduction electron contribution for the protons can be written,[29,48,58]

$$(T_{1,p}T)^{-1}=C_0[\chi_{ce}(T),\sqrt{\tau^*/\tau_\parallel}]g(\omega_e)+C_{2k_F}[\chi_{ce}(T)], \tag{8}$$

with

$$g(\omega_e)=\left(\frac{1+[1+(\omega_e\tau^*)^2]^{1/2}}{2[1+(\omega_e\tau^*)^2]}\right)^{1/2} \tag{9}$$

and

$$(\tau^*)^{-1}=(\tau_\perp)^{-1}+(\tau_{ce-d})^{-1}. \tag{10}$$

The temperature dependence of $\tau_\perp$ (hopping motion) follows an activation law,[29]

$$\tau_\perp(T)=C_\perp e^{\Delta E/(k_BT)}, \tag{11}$$

and the temperature dependence of τ_{ce-d} was explained by Pongs and Dormann.[13] The constants C_0 and C_{2k_F} in Eq. (8) are functions of the enhancement factors $K_0(\alpha)$ and $K_{2k_F}(\alpha)$ that are the result of the quasi-one-dimensional electron movement,

$$C_0=\frac{1}{2}\frac{4\pi k_B}{\hbar(g\mu_B)^2}\sqrt{\frac{\tau^*}{\tau_\parallel}}K_0(\alpha)\bar{A}_e^2\chi_{ce}(T)^2$$

$$C_{2k_F}=\frac{1}{2}\frac{4\pi k_B}{\hbar(g\mu_B)^2}K_{2k_F}(\alpha)\bar{A}_e^2\chi_{ce}(T)^2, \tag{12}$$

where A_e is the hyperfine field of the protons which can be estimated from the spin densities ρ_i determined above. We refer to Bourbonnais *et al.* for the corrected expression of the $2k_F$ contribution to Eq. (12).[59] This contribution is irrelevant for $(NA)_2AsF_6$, however. (See Table III.)

3. Anion rotation in the naphthalene salt

The temperature dependence of the fluorine spin-lattice relaxation rate shows at both Larmor frequencies two maxima between 70 and 250 K (Fig. 7) with a small distance

TABLE II. Fit parameter of the temperature dependence of the spin-lattice relaxation rate of the fluorine nuclei in $(NA)_2AsF_6$ at a Larmor frequency of 53 MHz and 282 MHz.

	K/s^{-2}	τ_∞/s	E/meV
	Fit parameter at 53 MHz		
FH	3.2×10^{8}	1.0×10^{-11}	79
FF	2.0×10^{9}	1.3×10^{-13}	133
	Fit parameter at 282 MHz		
FH	6.7×10^{8}	9.0×10^{-13}	96
FF	4.8×10^{9}	2.5×10^{-13}	105

between their centers of gravity. The structured maximum has been fitted with the above described theoretical BPP model independently at both frequencies (solid line, Table II). The motion-induced relaxation of the fluorine nuclei can be inferred from the shift of the position of these maxima to higher temperatures at a Larmor frequency of 282 MHz compared to the position at 53 MHz. The low-temperature maximum is caused by the interaction of fluorine nuclei and protons, whereas the maximum at higher temperatures results from the fluorine-fluorine interaction. If the high-frequency data are described by the parameters obtained from fitting the low-frequency results, the broken line is obtained (Fig. 7). Obviously the measured relaxation rate at the higher Larmor frequency is a factor 2 higher than predicted by the parameters gained at 53 MHz. In the BPP model the spectral density $J(\omega)$ of the rotational movement of the octahedra obeys a Debye form, meaning a statistical distributed movement of the anion octahedra. The deviating frequency dependence of T_1^{-1} is a hint of a not pure statistical distribution of the octahedral rotation jumps. A correlated movement of the octahedra is a reasonable explanation for the deviation of the spectral density from a Debye form. Nevertheless the position of the maxima can be correctly described by the BPP model and this gives credit to the relevant fit parameter, i.e., the correlation time of the motion, τ_c, and the activation energy of the rotational jumps E.

The temperature-independent but frequency-dependent contribution to the relaxation rate $T_{1,FD}^{-1}$ results from spin diffusion to paramagnetic defects. The observed frequency dependence is between fast diffusion $(1/\omega^2)$ and slow diffusion $(1/\sqrt{\omega})$, limiting behavior.[53–57] Such a contribution has also been observed in $(FA)_2X$ salts.[40]

The contribution to the fluorine rate, $T_{1,FH}^{-1}$, which results from the interaction between the fluorine nuclei and the protons, is also seen and should be described by the same fit parameters, regarding the temperature dependence, in the spin-lattice relaxation rate of the protons. The temperature dependence of $T_{1,H}^{-1}$ (Fig. 8) shows indeed the expected BPP maxima. There are again two maxima, one resulting from the ^{1}H-^{1}H interaction and the other resulting from the ^{1}H-^{19}F interaction. The maxima of the temperature dependence of the rate at the different Larmor frequencies are fitted simultaneously, using for the ^{1}H-^{19}F interaction the parameters gained by the fit of $T_{1,F}^{-1}(T)$ of the fluorine nuclei at 53 MHz. The fit shows a 10 K error of the maxima but describes the relative positions and the height correctly, which is a sign of the consistent description by the BPP model. A frequency-dependent offset, as seen before at the temperature dependence of the fluorine rate is also present and can be explained as above. For the protons at temperatures above the BPP maxima the Korringa relaxation via the conduction electrons has to be considered. In this high-temperature range, the influence of the paramagnetic defects, $T_{1,HD}^{-1}$, is reduced.

TABLE III. Fit parameters for conduction electron ^{1}H spin-lattice relaxation contribution in $(NA)_2AsF_6$. For the definition of the parameters see Sec. III B 2.

$\tau_\parallel$	4.69 fs
τ^* (240 K)	0.72 ns
$\tau_\perp$ (240 K)	0.79 ns
$C_\perp$	0.35 ns
ΔE	16.6 meV
τ_{ce-d} (240 K)	8.13 ns
C_0T (240 K)	67.86 s^{-1}
$C_{2k_F}T$ (240 K)	0.66 s^{-1}

4. Conduction electron spin dynamics

The conduction electron dynamics in this quasi-1D organic conductor can now be characterized by the quantitative description of proton T_1^{-1} in the high temperature range (Fig. 5). This enables us to determine the time constant τ^* (Sec. III B 2) in the form of a fit parameter. τ^* describes the mean time allowed for the quasi-1D diffusive decay of the long wavelength conduction electron spin correlation.

The frequency dependence was measured at 240 K so that the salt is still in the metallic phase (Fig. 9). In addition, this temperature is low enough that the salt is stable over a long time period and the contribution of the motion of the anion octahedra to the relaxation rate is negligible.[43] The temperature dependence of the longitudinal relaxation rate resembles accidentally a linear behavior above the Peierls transition temperature. The slope of the three curves (Fig. 5) measured at different Larmor frequencies can be simultaneously fitted using Eqs. (8) and (9) with only one parameter set. The increase of the rate to higher temperatures is Korringa-like and, due to the quasi-1D movement of the conduction electrons, the slope increases with decreasing Larmor frequency. An analysis of the $(PY)_{12}(SbF_6)_7$ radical cation salt showed[43,60] that τ^* results from two time constants: $\tau_\perp$,which is the transversal hopping time, and τ_{ce-d}, which is the time needed for the conduction electron to hit a defect spin [Eq. (10)]. The fit parameters for the temperature dependence of the transverse hopping motion, $(\tau_\perp)^{-1}$, i.e., $C_\perp$ and ΔE [Eq. (11)], are given in Table III. Whereas $(\tau_\perp)^{-1}$ increases with temperature (T), $(\tau_{ce-d})^{-1}$ decreases with increasing T due to the exponential decrease in the defect-conduction electron mutual exchange integral with increasing temperature and NA-molecular librational amplitude.[61] The different temperature dependences of $\tau_\perp$ and τ_{ce-d} and the temperature dependence of $\chi_{ce}(T)$ derived in Fig. 9 has to be taken into account for a simulta-

neous fit of the three temperature dependencies and the frequency dependence at 240 K of the proton longitudinal relaxation rate T_1^{-1} with the formula in Eq. (8). The scattering time $\tau_\parallel$ is taken approximately as constant in the temperature range examined. The fits are shown in Fig. 5 as a solid line. The parameters of the fit τ^*, C_0 and C_{2k_F}, are listed in Table III.

These empirical parameters actually are in quite reasonable agreement with their estimate according to Eq. (12). With help of the McConnell relation[62,63] and the spin density of the conduction electrons at the carbon sites (Table I) the hyperfine interaction constants A_e of the protons have been calculated. The LRA fit in Fig. 9 gives the Pauli susceptibility of $\chi_{Pauli,exp.}=160\times10^{-6}$ emu/mol. Assuming $\chi_{Pauli,theo.}=100\times10^{-6}$ emu/mol,[49] the enhancement factors are $K_0(\alpha)=0.78$ and $K_{2k_F}(\alpha)=4.33$ (Ref. 43). Thus it is possible to calculate the "isotropic" part of the parameters C_0 and C_{2k_F}. Considering dipolar interactions, in addition to Fermi contact hyperfine interactions,[64] the measured values agree with the theoretical values of C_0 and C_{2k_F}. The experimental ratio $C_0/C_{2k_F}\approx100$ underlines the enhancement of the Korringa rate due to the quasi-1D electron movement and justifies again the classification of $(NA)_2AsF_6$ as a quasi-1D conductor.

IV. DISCUSSION

A. Conduction electron spin density and dynamics

The radical cation salt $(NA)_2AsF_6$ shows the previously reported instability and is therefore difficult to handle. Nevertheless, sealed samples and the handling at temperatures below 250 K allowed us to measure the frequency and temperature dependence of the proton longitudinal relaxation rate and highly resolved ^{13}C spectra with nuclear magnetic resonance. The temperature dependence of the Knight shifts led to an intrinsic conduction electron susceptibility, which is more reliable than the integral results of SQUID measurements reported earlier (Fig. 9).

The assignment of the spectral lines to the carbon sites of the naphthalene molecules could be done with the help of gated decoupling measurements and the comparison with theoretical values of the line positions (Knight shifts). The unambiguous assignment enabled us to calculate the spin densities of the electron spins at the carbon sites of the naphthalene molecules in the naphthalene stacks (Table I).

A simultaneous fit of the temperature and frequency dependence of the proton longitudinal relaxation rate yields as one of the fit parameters the time constant $\tau^*=0.72$ ns describing the end of the diffusive period for the quasi-1D spin dynamics of the conduction electron at 240 K.

The fit parameters describing the enhancement of the proton longitudinal relaxation rate due to the quasi-1D movement of the conduction electrons are in good agreement with the values calculated using the measured spin density and the intrinsic conduction electron susceptibility. Thus, our work provides a consistent picture of the electron density and electron dynamics in the prototype radical cation salt $(NA)_2AsF_6$.

TABLE IV. Comparison of the activation energies of $(PY)_{12}(SbF_6)_7$ und $(NA)_2AsF_6$, derived at a Larmor frequency of 53 MHz, and correlation times $\tau_{c,H}(T_P)$ at the Peierls transition temperatures T_P of $(FA)_2AsF_6$ und $(FA)_2SbF_6$ (Ref. 40).

	$(NA)_2AsF_6$	$(PY)_{12}(SbF_6)_7$	$(FA)_2AsF_6$	$(FA)_2SbF_6$
T_P/K	234	116	176	166
E_{HF}/meV	79	22	172	224
E_{FF}/meV	133	59		
$\tau_{c,H}(T_P)$/s	5.1×10^{-10}	1.7×10^{-8}	5.1×10^{-10}	5.1×10^{-9}
$\tau_{c,F}(T_P)$/s	9.4×10^{-11}	1.5×10^{-9}		

B. Slowing down of anion rotation and Peierls transition

The measurements of the low-temperature spin-lattice relaxation rate of the fluorine nuclei and of the protons in $(NA)_2AsF_6$ reflect the rotational movement of the anion octahedra. The frequency dependence of the BPP maximum of the spin-lattice relaxation rate deviates from the Debye behavior and indicates a nonstatistical distribution of the rotational jumps of the anion octahedra, but instead correlated jumps. To investigate a recently suggested connection between the Peierls transition temperature T_P and the freezing-in of the rotation of the anion octahedra, the correlation time of the motion of the fluorine nuclei at the Peierls transition temperature is compared for different radical cation salts with AsF_6 and SbF_6 octahedra in Table. IV. The salts with AsF_6 octahedra show, in spite of their very different transition temperatures, the same correlation times $\tau_c(T_P)$ for the motion, each at its T_P. For the salts with SbF_6 octahedra the correlation times $\tau_c(T_P)$, even if differing by a factor of 3, are still of the same order of magnitude. Despite the few data the tendency of a small range of correlation times at the Peierls temperature for the salts with the same anion octahedra can be concluded. The Peierls transition occurs when the rotational movement of the octahedra reaches a certain relatively long correlation time which differs very little for different radical cation salts. This supports the picture that the freezing-in of the octahedra and the additional three-dimensional (3D) coupling is responsible for the occurance of the Peierls transition.

In spite of the broad variation of the activation energies for the anion rotation and arene libration of the respective radical cation salts, the correlation times observed around the actual Peierls temperature fall in a narrow range of 10^{-10}–10^{-8} s. The example of fluoranthene salts indicates that the activation energy is correlated with the size of the complex anion, be it PF_6, AsF_6, or SbF_6.[40] Thus, while electron-phonon coupling and the softening of the $2k_F$ phonons are the well-known ingredients of the Peierls transition in quasi-one-dimensional conductors,[16] this slowing down of the rotational motion of the anions seems required for the development of 2D correlation of the 1D-CDW fluctuations. According to the 3D superstructure wave vectors of the fluoranthene and perylene salts, which have been analyzed in detail up to now,[9,10] the 3D-CDW ordered low-temperature structure of these radical cation salts results from Coulomb correlations, and thus out of phase arrangement in the third direction, however.[37]

V. CONCLUDING REMARKS

We analyzed the naphthalene radical cation salt $(NA)_2AsF_6$, because it shows, from all quasi-one-dimensionally conducting arene salts studied up to now, the highest Peierls transition temperature T_P and the most pronounced influence of electron phonon coupling and CDW fluctuations on the static magnetic susceptibility.[15] By a detailed NMR analysis, the intrinsic, temperature-dependent conduction electron susceptibility $\chi_{ce}(T)$ has been determined for $T > T_P$ as well as $T < T_P$ (Fig. 9). The spin density distribution derived from Knight shift analysis (Table. I) proves that the naphthalene radicals, which are stacked with 90° rotation of subsequent molecules (Fig. 1), pack with optimized density overlap (carbon sites C1, C4, C5, and C8, Table I). The proton spin-lattice relaxation in the metallic phase of $(NA)_2AsF_6$ proves the highly one-dimensional character of this organic conductor by the enhancement of the long wavelength contributions, i.e., $C_0/C_{2k_F} \approx 100$ and by the anisotropy of the scattering times, i.e., $\tau^* : \tau_\parallel \approx 10^5 : 1$ (Table III).

According to earlier reasoning, the high T_P value might be linked to the anions being comparably tightly squeezed between the neighboring naphthalene stacks, with their common high-temperature rotation frozen-in at correspondingly high temperatures.[36] This was indeed substantiated in the experimental analysis presented here.

The correlation between the Peierls transition and the occurance of a maximum of the fluorine nuclear spin-lattice relaxation rate could be supported by $(NA)_2AsF_6$ as in the other radical cation salt studied before. The temperature dependence of the low-temperature spin-lattice relaxation rate of the protons shows a BPP-like behavior as well. The proton $T_{1,H}^{-1}$ maxima could be described with the fit parameters of the fluorine rates.

The correlation time of the anion rotational movement at the Peierls transition temperature, $\tau_c(T_P)$, is useful for a comparison of different radical cation salts. Salts with strongly different Peierls transition temperatures, with the same and with different anion octahedra, show only a small range of $\tau_c(T_P)$. [Salts with the same anion octahedra have almost the same $\tau_c(T_P)$.] The qualitative picture that the slowdown or freezing-in of the anion octahedra trigger the Peierls transition through the additional 3D coupling of the 1D-CDW fluctuations could be supported. Expressed the other way around, the low-temperature locked-in CDW-Peierls distorted phase of the quasi-one-dimensionally conducting arene salts is evidently prevented by substantial rotational motion of the complex anions, as it is also prevented by static anion chain disorder.[35]

ACKNOWLEDGMENTS

We thank I. Odenwald for crystal growth, H.-J. Koo and M.-H. Whangbo for extended Hückel tight-binding electronic band structure calculations, G. Fischer and B. Pongs for experimental contributions, and C. Buschhaus for discussions. This project was supported by the Deutsche Forschungsgemeinschaft.

[1] H. P. Fritz, H. Gebauer, P. Friedrich, P. Ecker, R. Artes, and U. Schubert, Z. Naturforsch. B **33b**, 498 (1978).
[2] Ch. Kröhnke, V. Enkelmann, and G. Wegner, Angew. Chem. **92**, 941 (1980).
[3] V. Enkelmann and K. Göckelmann, Ber. Bunsenges. Phys. Chem. **91**, 950 (1987).
[4] H. J. Keller, D. Nöthe, H. Pritzkow, D. Wehe, M. Werner, P. Koch, and D. Schweitzer, Mol. Cryst. Liq. Cryst. **62**, 191 (1980).
[5] V. Enkelmann, Adv. Chem. Ser. **217**, 177 (1988).
[6] W. Riess, W. Brütting, and M. Schwoerer, Synth. Met. **55-57**, 2664 (1993).
[7] C. Math, W. Brütting, and W. Riess, Europhys. Lett. **35**, 221 (1996).
[8] D. Berner, V. M. Burlakov, G. Scheiber, K. Widder, H. P. Geserich, J. Gmeiner, and M. Schwoerer, Solid State Commun. **97**, 863 (1996).
[9] V. Ilakovac, S. Ravy, J. P. Pouget, W. Riess, W. Brütting, and M. Schwoerer, J. Phys. IV **3**, C2-137 (1993).
[10] C. Buschhaus, R. Moret, S. Ravy, and E. Dormann, Synth. Met. **108**, 21 (2000).
[11] C. Hauenschild, J. W. Helberg, W. Riess, W. Brütting, and M. Schwoerer, Synth. Met. **55-57**, 2635 (1993).
[12] R. Desquiotz, M. Hofmann, and E. Dormann, Eur. Phys. J. B **16**, 403 (2000).
[13] B. Pongs and E. Dormann, Phys. Rev. B **65**, 144451 (2002).
[14] U. Köbler, J. Gmeiner, and E. Dormann, J. Magn. Magn. Mater. **69**, 189 (1987).
[15] B. Pongs, G. Fischer, and E. Dormann, J. Phys.: Condens. Matter **14**, 8655 (2002).
[16] D. Jerome and H. J. Schulz, Adv. Phys. **31**, 299 (1982).
[17] G. Sachs, W. Stöcklein, B. Bail, E. Dormann, and M. Schwoerer, Chem. Phys. Lett. **89**, 179 (1982).
[18] E. Dormann, Phys. Bl. **39**, 220 (1983).
[19] E. Müller, J. U. von Schütz, and H. C. Wolf, J. Phys. Colloq. **44**, C3, 1401 (1983).
[20] E. Dormann, G. Sachs, W. Stöcklein, B. Bail, and M. Schwoerer, Appl. Phys. A: Solids Surf. **30**, 227 (1983).
[21] E. Dormann, G. Denninger, G. Sachs, W. Stöcklein, and M. Schwoerer, J. Magn. Magn. Mater. **54-57**, 1315 (1986).
[22] H. Gebhardt and E. Dormann, J. Phys. E **22**, 321 (1989).
[23] M. Mehring, in *Low-Dimensional Conductors and Superconductors*, edited by D. Jerome and L. G. Caron (Plenum, New York, 1987), p. 185.
[24] G. Denninger, Adv. Solid State Phys. **30**, 113 (1990).
[25] R. Ruf, N. Kaplan, and E. Dormann, Phys. Rev. Lett. **74**, 2122 (1995); **75**, 1237 (1995).
[26] G. Alexandrowicz, T. Tashma, A. Feintuch, A. Grayevsky, E. Dormann, and N. Kaplan, Phys. Rev. Lett. **84**, 2973 (2000).
[27] T. Wokrina, J. Gmeiner, N. Kaplan, and E. Dormann, Phys. Rev.

B **67**, 054103 (2003).
[28] E. Müller, J. U. von Schütz, and H. C. Wolf, Mol. Cryst. Liq. Cryst. **93**, 407 (1983).
[29] G. Soda, D. Jerome, M. Weger, J. Alizon, J. Gallice, H. Robert, J. M. Fabre, and L. Giral, J. Phys. (Paris) **38**, 931 (1977).
[30] H. P. Geserich, B. Koch, W. Ruppel, R. Wilckens, D. Schweitzer, V. Enkelmann, G. Wegner, G. Wieners, and H. J. Keller, J. Phys. Colloq. **44** C3-1461 (1983).
[31] Th. Schimmel, B. Koch, H. P. Geserich, and M. Schwoerer, Synth. Met. **33**, 311 (1989).
[32] J. Wosnitza, *Fermi Surfaces of Low Dimensional Organic Metals and Superconductors* (Springer, Heidelberg, 1996).
[33] F. Nad, P. Monceau, C. Carcel, and J. M. Fabre, J. Phys.: Condens. Matter **13**, L717 (2001).
[34] K. Sengupta and N. Dupuis, Phys. Rev. B **65**, 035108 (2001).
[35] C. Buschhaus, R. Desquiotz, K. Eichhorn, M. Hofmann, K. Hümmer, V. Illich, M. Kelemen, S. Tarragona Auga, T. Wokrina, A. Zitsch, and E. Dormann, Eur. Phys. J. B **8**, 57 (1999).
[36] A. Kaiser, B. Pongs, G. Fischer, and E. Dormann, Phys. Lett. A **282**, 125 (2001).
[37] R. Desquiotz, Ph.D. thesis, Universität Karlsruhe, 1997.
[38] G. Fischer and E. Dormann, Phys. Rev. B **58**, 7792 (1998).
[39] W. F. Kuhs, G Mattern, W. Brütting, H. Dragan, M. Burggraf, B. Pilawa, and E. Dormann, Acta Crystallogr., Sect. B: Struct. Sci. **50**, 741 (1994).
[40] W. Höptner, M. Mehring, J. U. von Schütz, H. C. Wolf, B. S. Morra, V. Enkelmann, and G. Wegner, Chem. Phys. **73**, 253 (1982).
[41] G. Nemec, V. Illich, and E. Dormann, Synth. Met. **95**, 149 (1998).
[42] A. Abragam, *Principles of Nuclear Magnetism* (Clarendon Press, Oxford, 1989).
[43] A. Kaiser, Ph.D. thesis, Universität Karlsruhe (TH), Cuvillier, Göttingen, 2003.
[44] N. Bloembergen, E. M. Purcell, and R. V. Pound, Phys. Rev. **73**, 679 (1948).
[45] S. Leyer, R. G. Barnes, C. Buschhaus, G. Fischer, B. Pilawa, B. Pongs, A. Tinner, and E. Dormann J. Phys.: Condens. Matter **16**, 6147 (2004).
[46] D. Köngeter and M. Mehring, Phys. Rev. B **39**, 6361 (1989).
[47] K. F. Thier and M. Mehring, Phys. Rev. B **50**, 2142 (1994).
[48] M. Helmle and M. Mehring, in *Nuclear Spectroscopy on Charge Density Wave Systems*, edited by T. Butz (Kluwer Academic Publishers, Dordrecht, 1992), p. 275.
[49] H.-J. Koo and M.-H. Whangbo (private communication).
[50] M. Karplus and G. K. Fraenkel, J. Chem. Phys. **35**, 1312 (1961).
[51] A. Carrington and A. D. McLachlan, *Introduction to Magnetic Resonance* (Harper&Row, New York, 1969), Chap. 6.
[52] P. Lee, T. Rice, and P. Anderson, Phys. Rev. Lett. **31**(7), 462 (1973).
[53] N. Bloembergen, Physica (Amsterdam) **25**, 386 (1949).
[54] H. Rohrschach, Physica (Utrecht) **30**, 38 (1964).
[55] W. Blumberg, Phys. Rev. **119**, 79 (1960).
[56] G. Kurtsishvili, Sov. Phys. Usp. **8**, 743 (1966).
[57] P. D. Gennes, J. Phys. Chem. Solids **7**, 345 (1958).
[58] G. Sachs and E. Dormann, Synth. Met. **25**, 157 (1988).
[59] C. Bourbonnais, P. Wzietek, D. Jerome, F. Creuzet, L. Valade, and P. Cassoux, Europhys. Lett. **6**, 177 (1988).
[60] A. Kaiser, T. Wokrina, B. Pongs, and E. Dormann, J. Phys.: Condens. Matter **15**, 7085 (2003).
[61] B. Pongs and E. Dormann, J. Phys.: Condens. Matter **15**, 5121 (2003).
[62] H. McConnell and D. B. Chesnut, J. Chem. Phys. **28**, 51 (1958).
[63] H. McConnell and D. B. Chesnut, J. Chem. Phys. **28**, 107 (1958).
[64] F. Devreux and M. Nechtstein, *Quasi One-Dimensional Conductors*, edited by S. Barisic, Lecture Notes in Physics Vol. 95 (Springer, Berlin, 1979).